Electronic Supplementary Information

SELF-ASSEMBLY IN SYSTEMS BASED ON L-CYSTEINE–SILVER-NITRATE AQUEOUS SOLUTION: MULTISCALE COMPUTER SIMULATION

Maxim D. Malyshev,[a] Svetlana D. Khizhnyak,[a] Lubov V. Zherenkova,[a] Pavel M. Pakhomov[a] and Pavel V. Komarov [*ab]

[a] *Department of Physical Chemistry and General Physics, Tver State University, Tver, 170100, Russia.*
[b] *A.N. Nesmeyanov Institute of Organoelement Compounds RAS, Moscow, 119991, Russia.*

[*]*E-mail: pv_komarov@mail.ru*

Here we present the main experimental and additional computer simulation data on the system under study

S1. Experimental Details

A supramolecular system based on aqueous solutions of the amino acid L-cysteine HS-CH_2-CH(NH_2)-C(O)OH (L-Cys) and silver nitrate ($AgNO_3$), which can form thixotropic hydrogels at low concentrations of the initial components (~0,01%) was described in our works [1-3]. The practical importance of this gel system, consisting of biologically active compounds, is connected with an opportunity to apply it as a matrix for producing highly efficient pharmaceutical formulations. The simplicity of gelation in a low-concentration aqueous solution of L-cysteine–$AgNO_3$ is its main and attractive feature from an experimental point of view, it could be considered a one-pot procedure. First, two aqueous solutions of the initial compounds L-cysteine (3 mM) and $AgNO_3$ taken in excess (Ag^+/L-Cys = 1.25 - 1.29) are poured together, stirred vigorously, and left to stand for a while for aging. As a result, a transparent slightly yellow solution is formed, the so-called cysteine-silver solution (CSS). The addition of various electrolytes (sulfates, chlorides, and others) into the CSS initiates gelation. The concentration of the electrolytes in the CSS-based hydrogels is about 10 times lower than the L-cysteine concentration.

Despite the simplicity of the gelation procedure from the first view, experimental data [1-5] indicate that self-assembly in CSS is a multistage process. In the first stage, when aqueous solutions of L-cysteine and silver nitrate are mixed, the hydrogen atom of the thiol group is replaced by silver, resulting in the formation of silver mercaptide (SM) in the zwitterionic form AgS-CH_2-CH(NH_2^+)-C(O)O^- [5] (see Fig. S1). The reaction between L-cysteine and silver salt through the thiol group is confirmed by FTIR spectroscopy. In the spectra of CSS hydrogels with various electrolytes (Fig. S2), one can notice the absence of an absorption band at 2551 cm^{-1}, which corresponds to the

stretching vibrations of the SH group (marked with an arrow in the spectrum). The absence of the SH absorption band in the CSS spectrum was shown earlier in our work [6]. Moreover, after the mixing of silver nitrate and L-Cys solutions, the pH of the system drops to a value of 3, indicating the release of the H^+ protons. We emphasize that the interaction of cysteine and silver nitrate directly via the thiol group is also noted in Refs. [7-9].

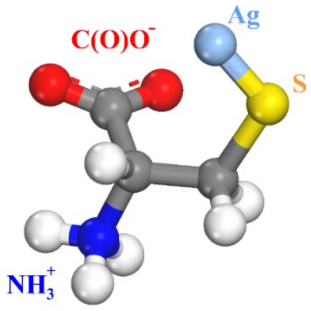

Fig. S1. The structure of silver mercaptide zwitterion.

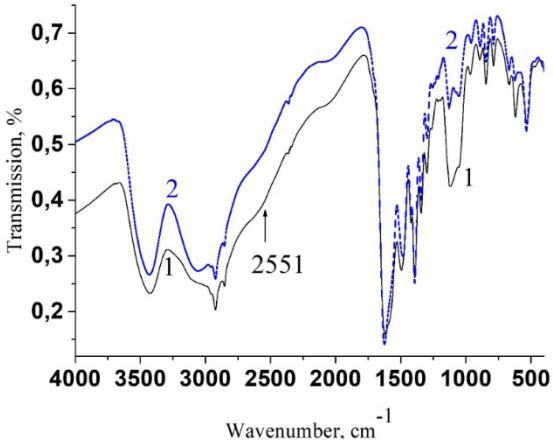

Fig. S2. FTIR spectrum of CSS/Na_2SO_4 (1) and CSS/NaCl (2) gel samples dried in liquid N_2.

At the next stage, during CSS maturation, according to UV spectroscopy data, SM cluster chains are formed. After mixing the initial components, two absorption bands (~312 and 390 nm) appear in the electronic spectrum of CSS (Fig. S3). To clarify the nature of the bands we changed first the concentration of L-Cys from 3.0 to 4.0 mM at a constant molar ratio of Ag^+/L-Cys = 1.25 (Fig. S3a,b) and then varied the molar ratio of Ag^+/L-Cys from 1,24 to 1,27 at a constant concentration of L-Cys equal to 3.0 mM (Fig. S3c,d). An increase in L-Cys content at a constant L-Cys/Ag^+ molar ratio leads to a growth in the intensity of both absorption bands; it should be noted that no shift in the maxima of the absorption band is observed (Fig. S3a,b). It means that the very concentration of the initial components (L-Cys and silver salt) affects the length and concentration of the SM cluster chains, the number of S-Ag bonds arising from charge transfer (~312 nm), and the formation of silver mercaptide clusters with the structure of the core-shell (390 nm).

Increasing the molar ratio of Ag^+/L-Cys at a constant concentration of L-Cys leads to another result - a slight drop in intensity of the absorption band at 312 nm and a shift of the maximum at 390 nm toward longer wavelengths are observed in the UV spectra (Fig. S3c,d). The shift of the maximum confirms our assumption that SM clusters with the "core-shell" structure are formed in the CSS, indicating an enlargement of the core of the clusters and some increase in their concentration, since there is also a slight growth of intensity of the absorption band at 390 nm.

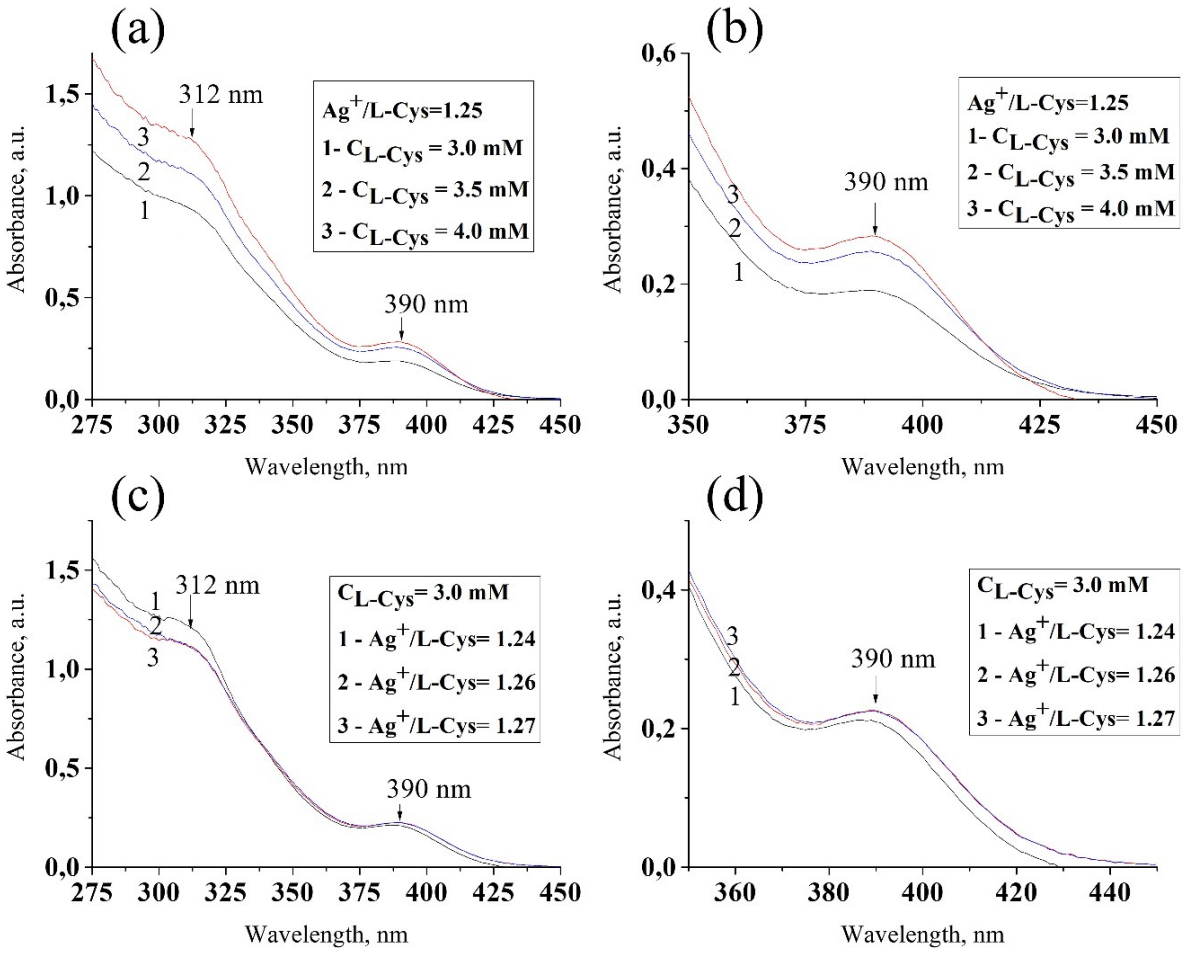

Fig. S3. UV spectra of CSS solutions in dependence of concentration and molar ratio of the initial components: a, b - C_{Cys} = 3.0, 3.5, 4.0 mM at a molar ratio of Ag^+/L-Cys = 1.25; c, d - molar ratio of Ag^+/L-Cys = 1.24, 1.26, 1.27 C_{Cys} = 3.0 mM.

The Dynamic Light Scattering (DLS) demonstrates the formation of SM clusters, the size of which depends on the concentration of the initial components (Fig. S4a,b). The figure shows particle size distributions in the CSS sample with a molar ratio of Ag^+/L-Cys = 1.23 at various dilutions: 1:2 (Fig. S4a) and 1:4 (Fig. S4b). The dilution was carried out at the CSS preparation stage, by adding to the sample the volume of water calculated according to the procedure [6] to reduce the concentration of the initial components 2 and 4 times, respectively. This led to a noticeable decrease in aggregate sizes because the concentration of the initial components changed at the time of the chemical interaction between the amino acid and the silver salt and subsequent self-assembly of the resulting supramonomers - SM molecules. As we can see from Figs.

S4a,b, a bimodal distribution of particles in the CSS is observed, indicating the formation of two types of clusters. Particles of smaller sizes can be called clusters (nuclei), from which larger aggregates are formed. Dilution of CSS leads to a decrease of the nucleus cluster sizes from 25 to 14 nm, and aggregates from 142 to 91 nm, which confirms the supramolecular nature of cluster chains consisting of SM molecules.

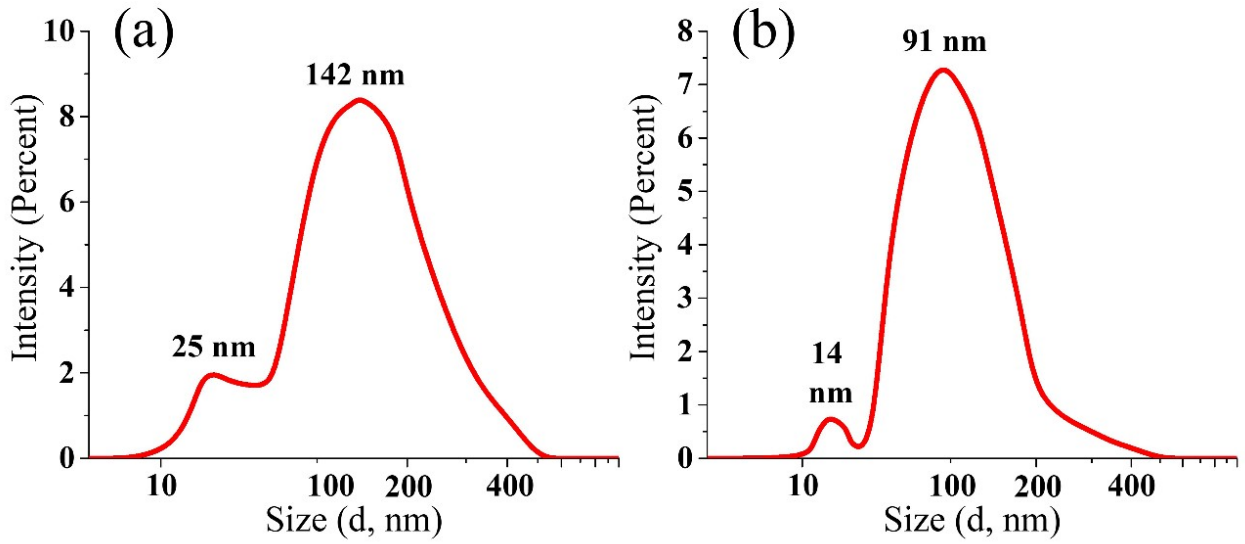

Fig. S4. Particle size distributions in the CSS with a molar ratio of Ag^+/L-Cys = 1.23: a - C_{Cys} = 1.5 mM (dilution 1:2), b – C_{Cys} = 0.75 mM (dilution 1:4).

According to electrophoretic light scattering data, the zeta potential of the SM clusters has a positive value, which depends on the concentration of the initial components (Fig. S5a,b). For example, the zeta potential of diluted CSS samples 2 and 4 times diluted is 61 and 48 mV.

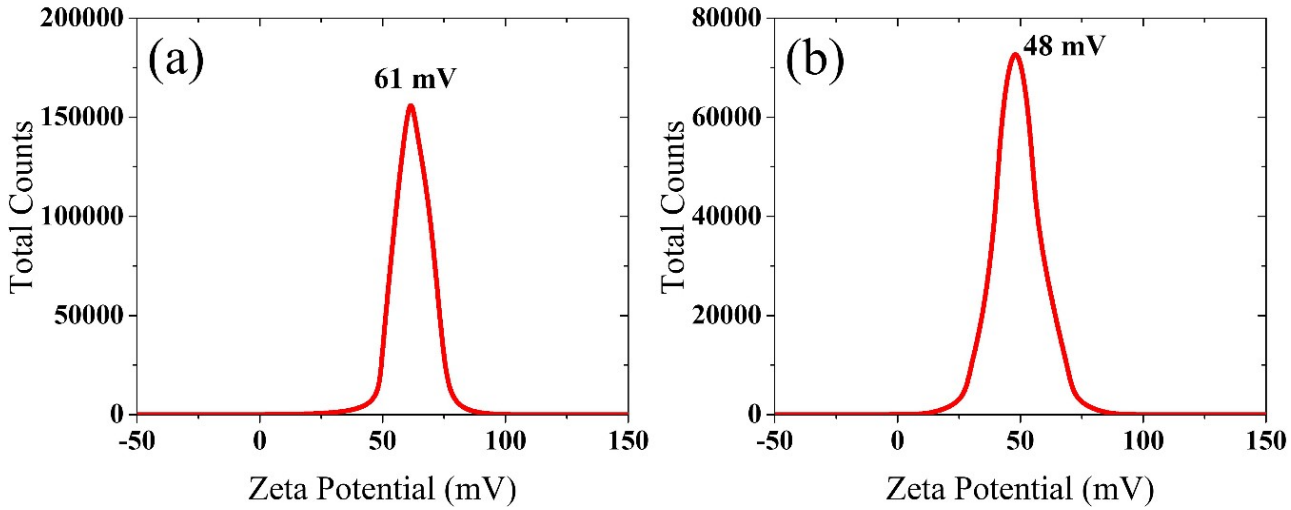

Fig. S5. Distributions of the zeta potential in the CSS with molar ratio of Ag^+/L-Cys = 1.23: a - C_{Cys} = 1.5 mM (dilution 1:2), b – C_{Cys} = 0.75 mM (dilution 1:4).

After mixing the solutions of the initial components and completing the aging stage, which varies from 30 minutes to 48 hours depending on the temperature, gelation

of the CSS is possible through the addition of low-molecular-weight salts of various metal electrolytes. It should be noted that gelation can occur at a rather low concentration of the dispersed phase (~0.01%). Transmission electron microscopy (TEM) shows how the morphology of the CSS changes after the addition of an electrolyte - the initiator of gelation (Fig. S6a,b,c). Fig. S6a shows the SM cluster chains that are transformed into fibers of a 3D network (Fig. S6b) under the influence of the electrolyte. The gel network fibers are seen to consist of discrete clusters with an average diameter of about 2.7 ± 1.9 nm (Fig. S6c). The estimation of cluster sizes is done using the ImageJ program [10]. The blackening in the electron micrograph is believed to be silver nanoparticles or silver sulfide crystals produced by the electron beam. The latter is possible if the silver atoms in the gel network fibers form compact structures.

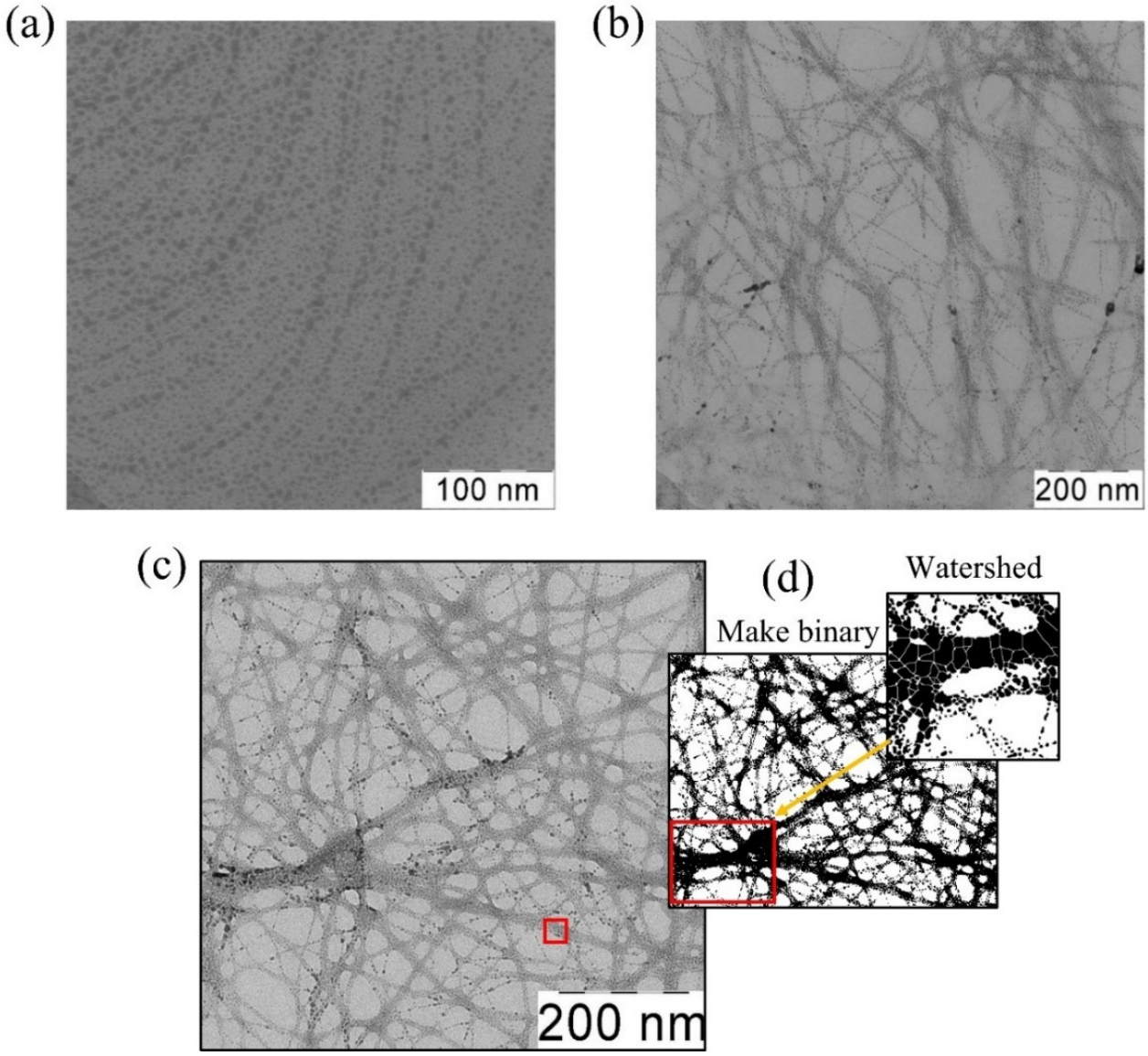

Fig. S6. TEM images of the CSS (a), CSS/$CuSO_4$ (b) (Ccys – 0.75 mM, C_{AgNO3} – 0.95 mM, C_{CuSO4} – 0.05 mM) and CSS/Na_2SO_4 (c) samples (C_{Cys} = 3.0 mM, C_{AgNO3} = 3.75 mM, C_{Na2SO4} = 0.2 mM); (d) processing of TEM images using the ImageJ [10].

When an electrolyte is added to the CSS, the electrostatic stabilization of the aggregates is disturbed, which initiates their self-assembly into the three-dimensional gel network. According to DLS data, immediately after adding the electrolyte ($CuSO_4$) to CSS, the cluster size decreases from 44 to 8 nm, which is clearly shown in the size distribution of the particles in units of volume of the scattering particles (Fig. S7). However, after some time (30 min, 2 hours), an increase in the size of the main scattering particles is recorded, 18 and 1473 nm. Thus, we observe the formation of fragments of the gel network. At the same time, there is also a noticeable increase in the size of large aggregates, marked with an arrow in Fig. S7, which makes the main contribution to light scattering.

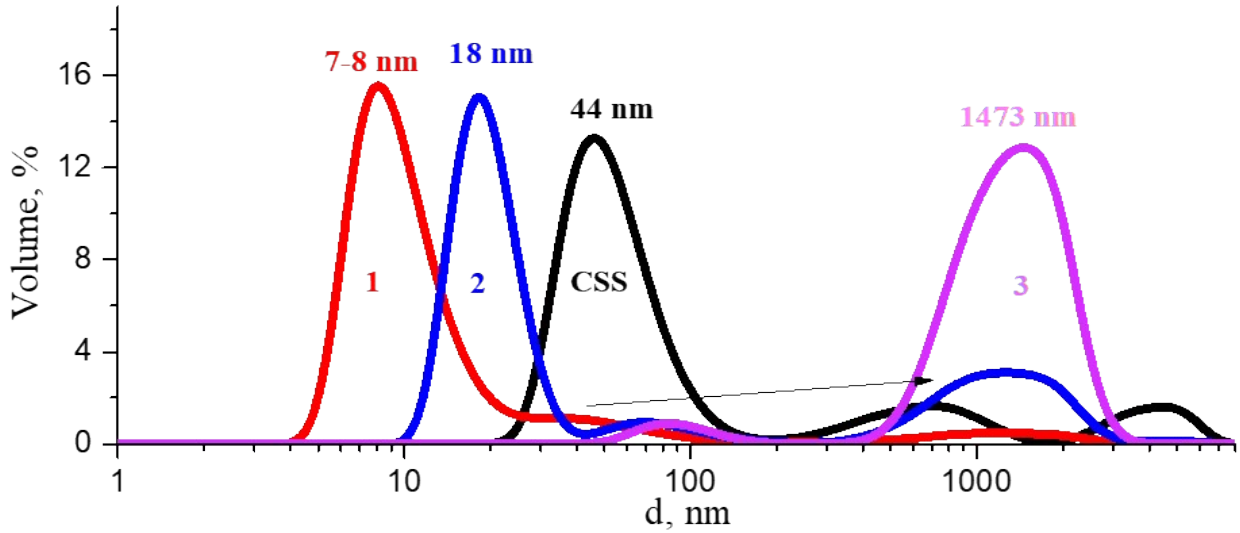

Fig. S7. Particle size distribution in CSS after addition of the $CuSO_4$ solution in dependence on time: 1 – 5, 2 – 30, 3 – 120 min. $C_{L\text{-}Cys}$ – 0.750 mM, C_{AgNO_3} – 0.953 mM, C_{CuSO_4} – 0.025 mM.

It is important to note that CSS gelation occurs in a narrow range of electrolyte concentrations. If there is a lack of an electrolyte, gelation doesn't take place, while exceeding a certain, critical a given electrolyte value can lead to precipitation (Fig. S8). As we see from the figure, immediately after the addition of the electrolyte, signs of microphase separation are noted in the sample with a high content of copper sulfate – *N*7 (see Fig. S8). The turbidity of the sample is evidence of the coagulation process. To observe the gelation process and to estimate stability over time of the hydrogel samples in dependence on the electrolyte concentration we can consider Fig. S8 by going from photos of the freshly prepared sample (a) to the stored ones during 1 day (b), 4 days (c), 9 days (d), and 14 days (e).

The gelation initiated by an electrolyte and the formation of the 3D network in a hydrogel over a period of time is confirmed by the results of the viscometry study. Fig. S9 demonstrates kinetic dependences of relative viscosity on time obtained for hydrogel #2 of the sample series shown in Fig. S8.

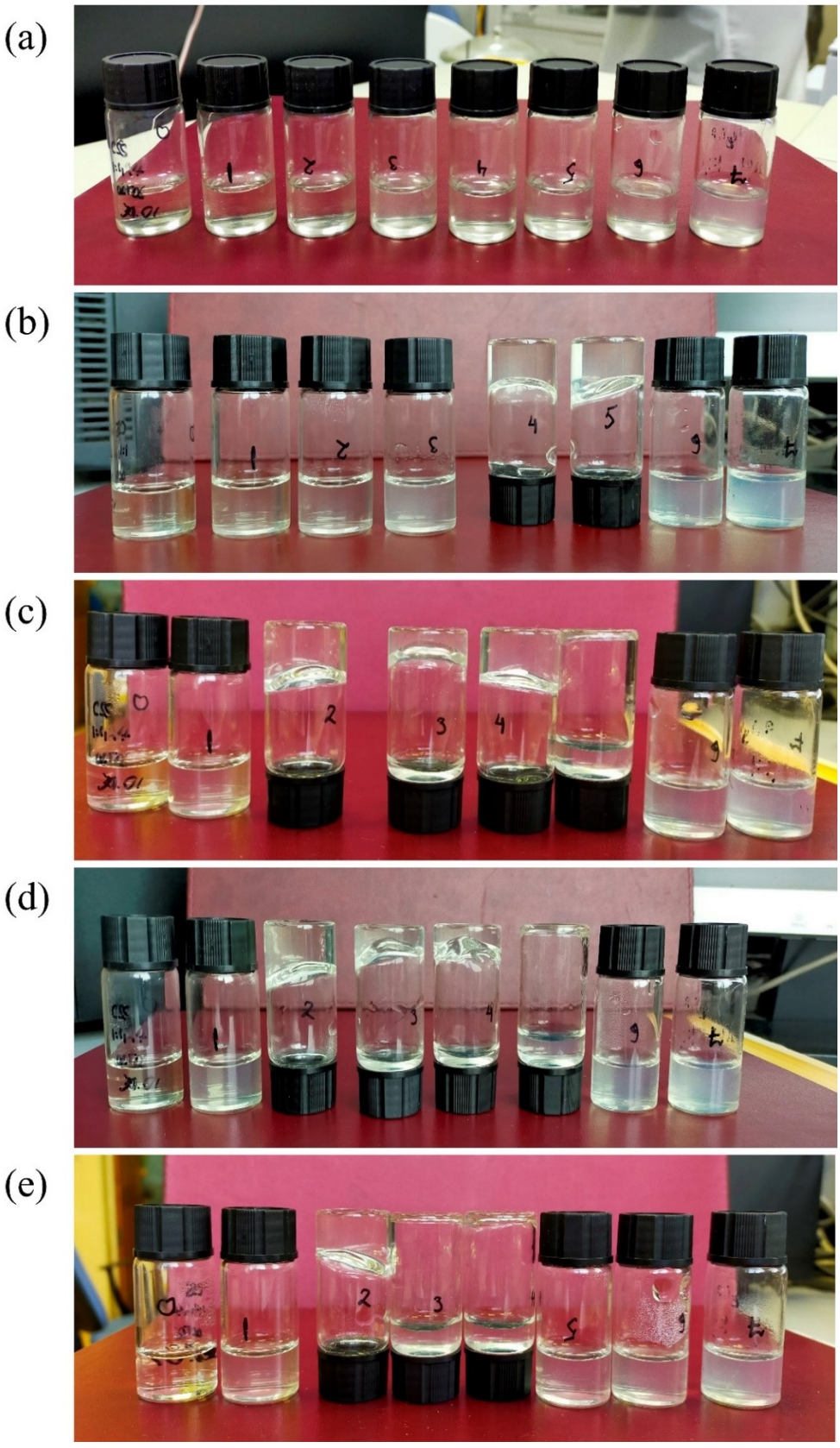

Fig. S8. Snapshot of CSS samples after the addition of various amounts of $CuSO_4$ solution (0.0, 0.01, 0.02, 0.025, 0.03, 0.035, 0.04, 0.05 ml of $CuSO_4$/1 ml CSS; from left to right: # 0–7) in dependence on time: (a) – freshly prepared, (b) – 1 day, (c) – 3 days, (d) – 6 days, (e) – 14 days. $C_{L\text{-}Cys}$ – 3.0 mM, C_{AgNO_3} – 3.8 mM.

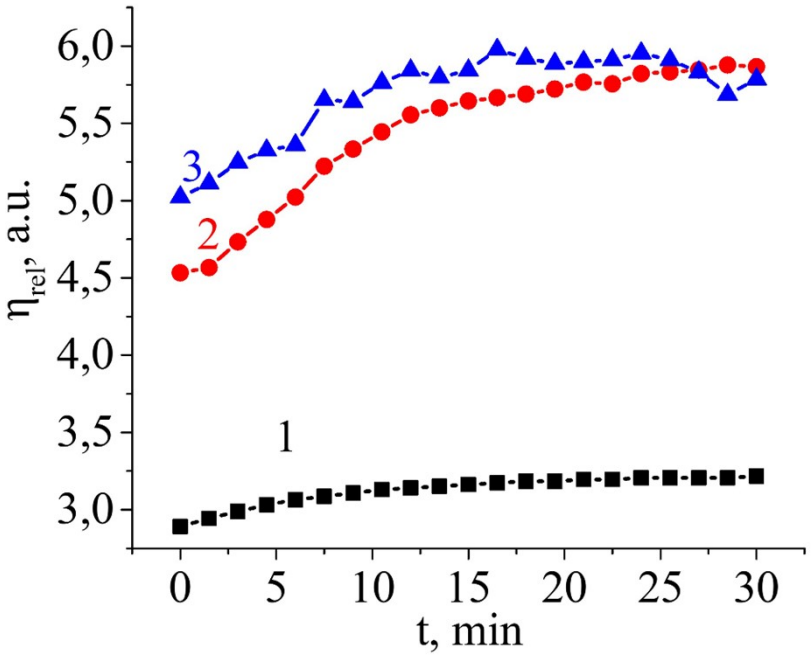

Fig. S9. Relative viscosity of the CSS/$CuSO_4$ (C_{CuSO4} - 0.2 mM, $C_{L\text{-}Cys}$ – 3.0 mM, C_{AgNO3} – 3.8 mM) hydrogel in dependence on time after addition of $CuSO_4$: 1 – 30 min, 2 – 3 days, 3 – 6 days.

As seen from Fig. S9, the relative viscosity of the sample increases with a time: of 30 minutes, 3, and 6 days after preparation (curves 1, 2, 3, respectively), and there is a monotonous increase of viscosity value during the measurement on the vibration viscometer. For comparison, the relative viscosity of CSS is ~1.3. Thus, we confirm not only the formation of the structure in the hydrogel sample but also the strengthening of the spatial network as a result of multiple intermolecular interactions.

S2. Complexation of Silver Mercaptide

Let us now discuss the features of complex formation by the SM zwitterions. To this end, we performed *ab-initio* calculations using the electron density functional theory (DFT) in the generalized gradient approximation (GGA) with the BLYP functional [11,12], basis DNP (double numerical with polarization) [13,14] using Gaussian [15]. The solvent was taken into account by setting the dielectric constant ε = 78.54.

The complexes formed by SM zwitterions with the CSS components (SM, water molecules, NO_3^- and Ag^+ ions) were considered (hydroxonium ions were not taken into account). Furthermore, we considered the complex formation of SM with SO_4^{2-} and Na^+ ions. Initial configurations were constructed according to the following scheme. The initial mutual arrangement of molecules and ions was generated at random. The distance between the nearest atoms of ions and the functional groups $C(O)O^-$, NH_3^+, and SAg of silver mercaptide varied in the range of 1 to 3 Å. Next, the total energy of the constructed system, E_α, was minimized (α is the type of complex) through geometric optimization.

During this stage, the generated arrangement of components was either slightly adjusted (while the binding energy of the system increased), or the given configuration was transformed into complexes of another type. The structures obtained were identified by the energy and the mutual arrangement of the functional groups of the system. The resulting stable complexes (not changed by repeated geometric optimization) are shown in Fig. S10, with their binding energy calculated using the following expression: $\Delta E_\alpha = |(E_\alpha - \sum E_{0,i})|$, where ΔE_α is the binding energy, E_α is the total energy of the system, $\sum E_{0,i}$ is the total energy of the noninteracting components.

Fig. S10 shows that the systems formed due to the interaction of SAg functional groups (complexes c_3 and c_6) have the highest binding energy. Since the interaction energy of S..Ag atoms make the largest contribution to the binding energy of SM complexes, and it is the SAg groups that play the most significant role in the formation and stabilization of nuclei of SM aggregates. This is indicated by the peculiarity of the localization of SAg functional groups at $N < 25$ (Fig. 3). In this case, thiol-silver oligomeric chains of the …AgS-AgS… type can be formed [16].

Consider complexes c_3 and c_6 in more detail. In the c_3 complex, the distance between the pairs of SAg atoms is about 2.7 Å, while a value of 3 Å characterizes the Ag-Ag pair. A similar structure in the case of the incorporation of the Ag^+ ion (complex c_6) is characterized by a considerable distance (4.6 Å) between the S and Ag atoms of the SM zwitterions. Nevertheless, the distances between the Ag^+ ion and S atoms of the SM are 2.5 Å, while Ag-Ag pairs (including Ag^+) coincide with the distance in the c_3 complex (3 Å). This suggests that the incorporation of silver ions is accompanied by little changes in the mutual arrangement of the S-Ag and Ag-Ag pairs. In addition, the incorporation of silver ions into SM clusters is energetically favorable (complexes of the c_6 type in Fig. S10). The properties of complexes c_3 and c_6 explain the formation of the "core-shell" structure for silver mercaptide clusters. At the same time, the binding energy of the a_7 complex points to a possible mechanism of cluster growth resulting from the bonding of carboxyl groups to SAg groups of the aggregating SM zwitterions.

The binding energies of complexes a_3, b_3, and d_3 are approximately equal (see Fig. S10) and correspond to the hydrogen bond energy. This confirms the assumption made in the previous section that multiple cross-linking of NH_3^+ and $C(O)O^-$ groups stabilize supramolecular structures formed by SM clusters. Furthermore, the presence of these functional groups on the surface of the clusters explains the ability of CSS-based hydrogels to bind a large number of water molecules (a_1, a_2, b_1, b_2, d_1, and d_2 complexes). Also, complexes with SO_4^{2-} and NO_3^- anions (b_4, b_5, b_7, c_1, c_2, c_4, and c_5) can potentially be formed in CSS, providing cross-linking of clusters and stabilization of supramolecular structures. Fig. S10 demonstrates the ability of SO_4^{2-} and NO_3^- anions to act as a binding agent between the SM zwitterions. Furthermore, in some cases, the binding energy of such complexes is much higher than when the NH_3^+ and $C(O)O^-$ groups are cross-linked. In the MD simulation (see Sect. 2.1), we did not take sulfate anions into account but observed the formation of a supramolecular aggregate. As for

the NO_3^- anions, they are localized on the surface of the SM clusters. The structures of complexes a_4, a_6, a_8, and c_6 demonstrate that metal ions formed due to salt dissociation are also capable of coordinating SM functional groups, which strengthens the bonding of SM clusters due to ionic bridges.

The performed calculations show that SM can form a wide variety of complexes, whose total energy contribution stabilizes supramolecular structures formed from SM clusters. In the following, we will see that the self-assembly of supramolecular aggregates at different length scales of order is determined precisely by the diversity of these complexes.

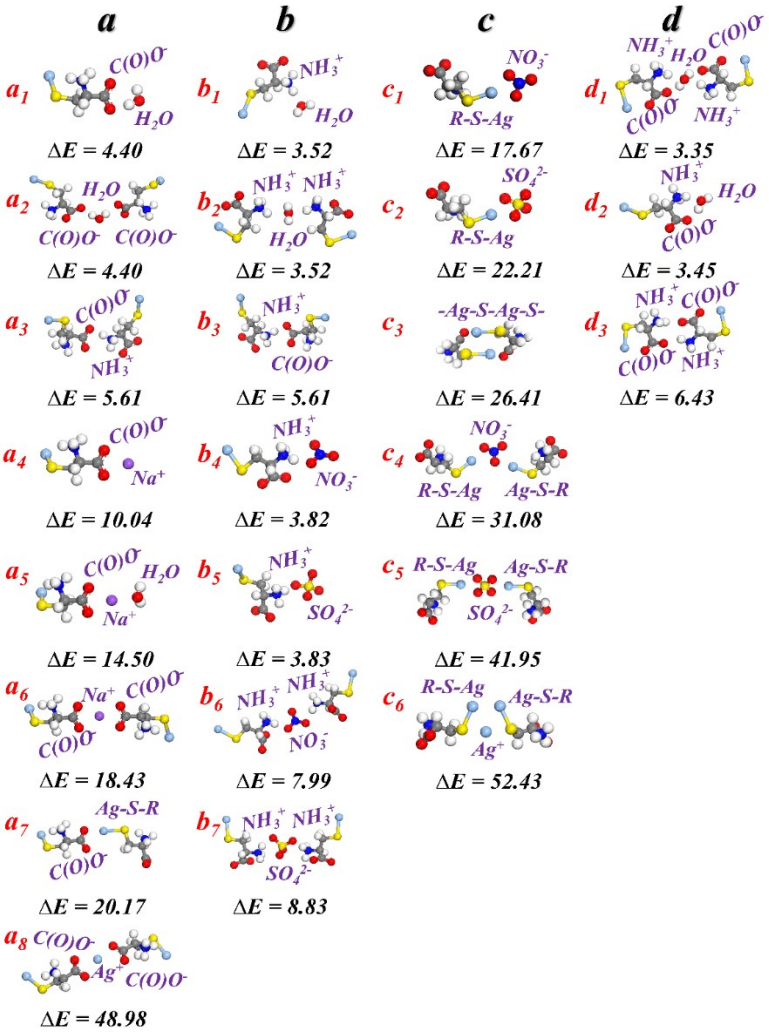

Fig. S10. Binding energies for complexes of silver mercaptide and various components. The letters *a*, *b*, *c*, and *d* define the functional groups involved in the intermolecular interaction with silver mercaptide: *a* – $C(O)O^-$; *b* – NH_3^+; *c* – SAg; *d* – NH_3^+ and $C(O)O^-$. The observed silver mercaptide complexes with various components of CSS (SM, NO_3^-, SO_4^{2-}, Ag^+, Na^+, H_2O) are indicated by letters with a subscript for convenience of description. The binding energy, ΔE, is presented in kcal/mol. Color designation of atoms: white balls correspond to hydrogen atoms, black - carbon, blue - nitrogen, red - oxygen, yellow - sulfur and blue – silver.

S3. Radial Distribution Function

We have used the following definition for the radial distribution function:

$$g_{\alpha\beta}(r) = \frac{N}{\rho N_\alpha N_\beta}\left\langle \sum_{i=1}^{N_\alpha}\sum_{j=1}^{N_\beta} \delta(r - r_i - r_j)|_{\alpha=\beta \Rightarrow i \neq j} \right\rangle \text{, (S1)}$$

where N_α is the number of atoms of chemical type α, N is the total number of atoms, ρ is the density of the system. The brackets < > indicate time or configurational averaging in the case of MD and MC simulations, respectively.

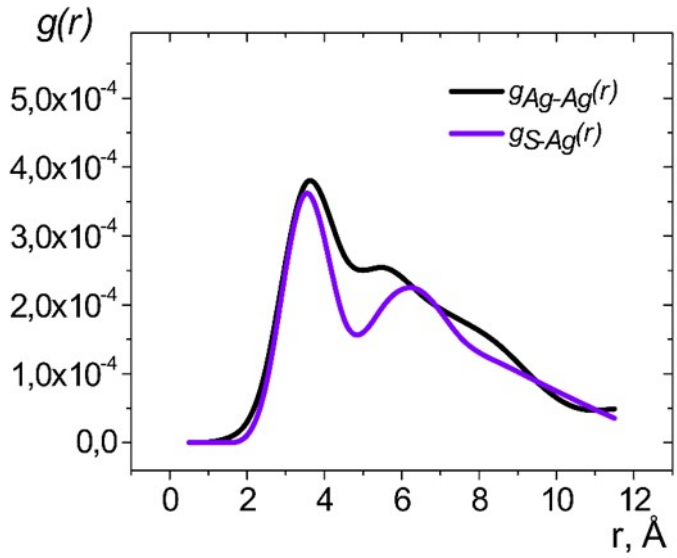

Fig. S11. Intermolecular radial distribution functions, *g*(r), for pairs of (a) S-Ag and (b) Ag-Ag atoms for the SM cluster (*N* = 22) prepared using MC simulation.

S4. Scaling Coarse-Grained Units to Real Units

Table S1. Summary of coarse-grained model parameters.

Parameter	Dimensionless units	Real units
Length (σ^*)	1	14 Å
Depth of the potential well at 300K (ε^*)	48	28.7 kcal/mol
Temperature (T^*)	1	300 K
Mass (m^*)	1	2736 amu ($4.6 \cdot 10^{-24}$ kg)
Friction coefficient (γ)	1-500 [1)]	$0.02 \cdot 10^{12}$–$10.71 \cdot 10^{12}$ c^{-1}
Energy ($k_B T^*$)	1	$414 \cdot 10^{-23}$ J

Time (τ)	1	46.7 · ps

[1)]The magnitude of the friction ($\gamma = k_B T^* / m^* D$, where D is particles diffusion coefficient) was varied within the indicated limits during testing of the CSS mesoscopic model. Since the value of this parameter only affected the speed of the self-assembly process, the value $\gamma = 1$ was used for subsequent simulations for reasons to accelerate the evolution of the system.

S.5. Parameterization of the Lennard-Jones potential

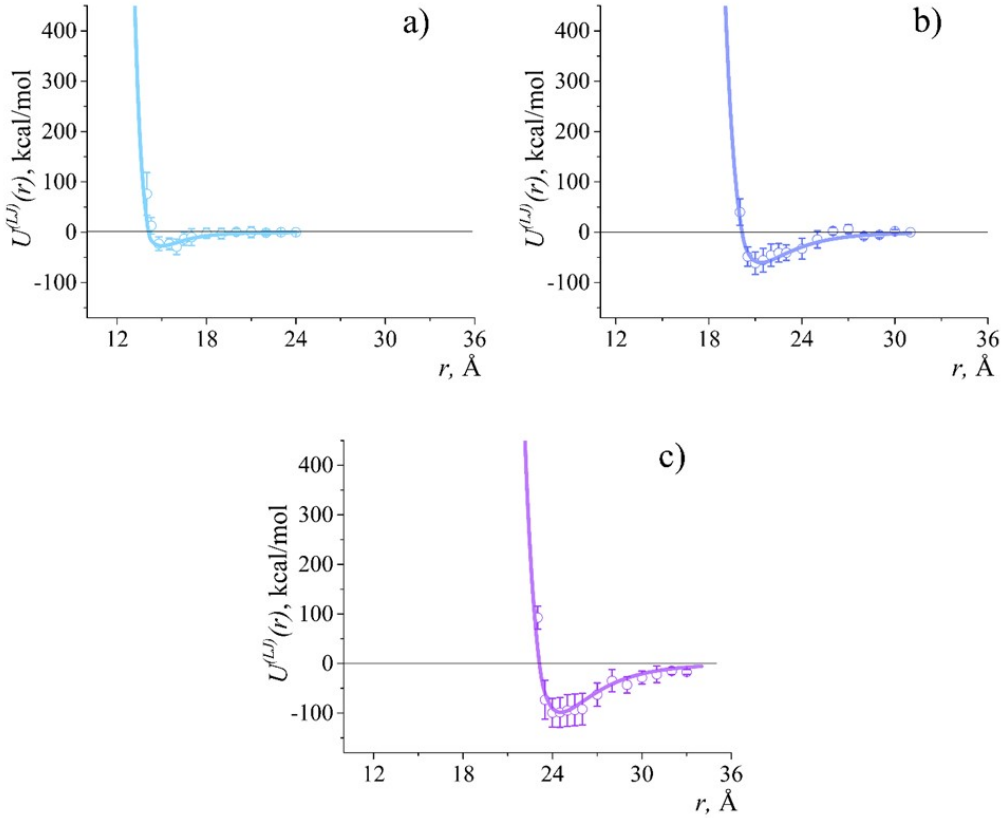

Fig. S12. The results of fitting Lennard-Jones potential, eq. (4), for pairs of SM clusters of different diameters σ_i in the case when $m = 22$, $n = 11$: a) $\sigma_1 = 14$ Å; b) $\sigma_2 = 20$ Å; c) $\sigma_3 = 23$ Å.

S6. Contact Area of SM Clusters

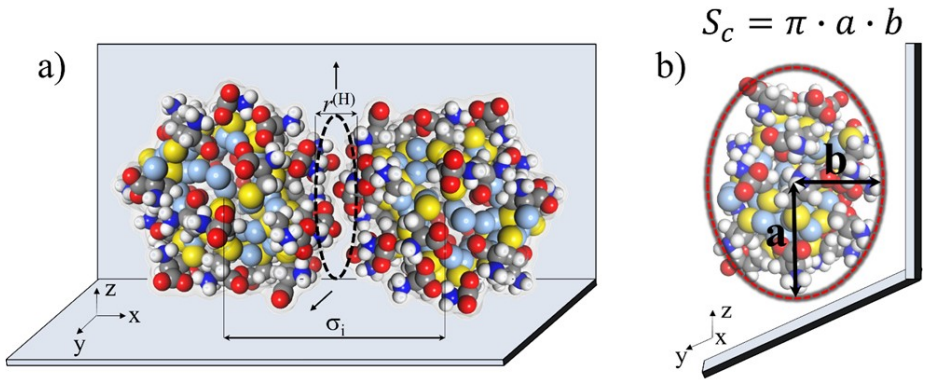

Fig. S13. Estimation of the area of the contact zone S_c. The following designations are used here: $r^{(H)}$ is the length of the hydrogen bond, σ and is the diameter of the cluster used for parameterization of potential (4).

When constructing the intermolecular interaction potential of the clusters (4), we proceeded from the assumption that it should have a short-range character and depend on the number of atoms located directly in the contact zone of the cluster surfaces, see Fig S13. We refer to the contact zone as atoms located on the surface of clusters, the distance between which: i) is not less than the sum of vdW radii (which were taken from the parametrization of the PCFF valence force field [17]), and ii) does not exceed the hydrogen bond length ($r^{(H)}$), which was chosen equal to $r^{(H)}$ = 2.2 Å [18] for estimates.

S7. On Probability of Formation of Filamentary Morphology in CSS Coarse-Grained Model

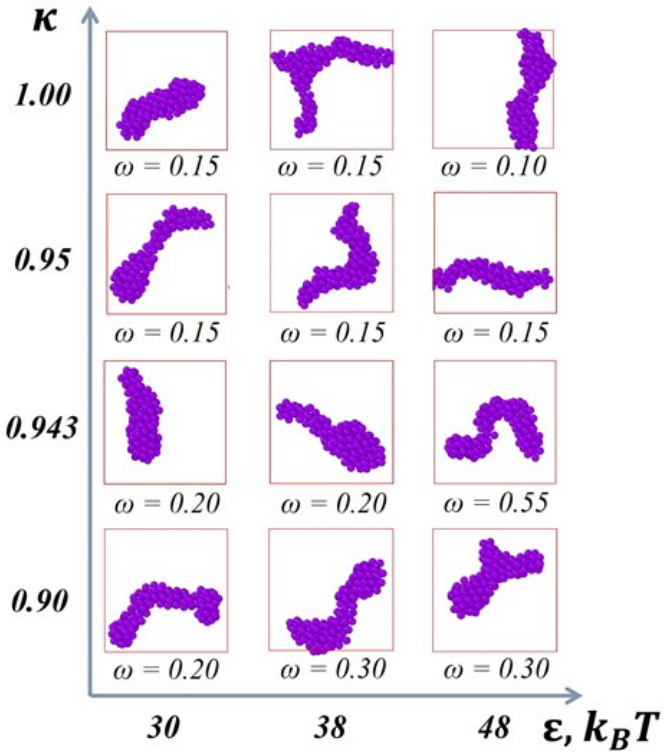

Fig. S14. Probability of filamentary morphology formation in a narrow range of model parameters (κ, ε).

S8. On Reversibility of the Supramolecular SM Aggregates in Atomistic Model of CSS

To check the reversibility of the SM aggregates obtained using the full atomistic CSS model, we conducted an additional MD simulation. As the initial state, we used the final state shown in Fig. 1. The simulation was carried out at constant temperature T=330 K using the same methodology as described in Sect. 2.1. The temperature increase was carried out smoothly for 2.5 ns. Fig. S15 shows a fairly fast disassembling of the filament-like aggregate which is a common feature of supramolecular systems. In this way, this result confirms the temperature reversibility of our atomistic CSS model.

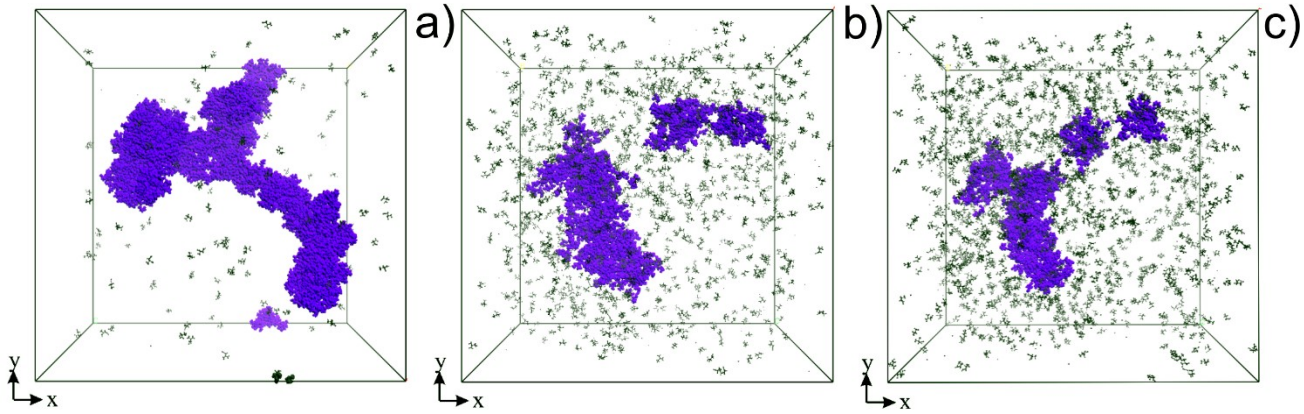

Fig. S15. Snapshots of the distribution of SM zwitterions at T = 340 K for different simulation times: a) 0 ns, b) 5 ns, and c) 10 ns. The other components of the atomistic model of CSS vanished for easier visualization. The edge of the simulation box is equal to 21.5 nm. The state of the CSS model shown in Fig. 1 was used as an initial state (0 ns). Aggregates of silver mercaptide are highlighted in blue, unbound SM zwitterions are given in gray.

References

1. P. M. Pakhomov, M. M. Ovchinnikov, S. D. Khizhnyak, M. V. Lavrienko, W. Nierling, M. D. Lechner, *Colloid J.,* 2004, **66**, 73-79.
2. P. M. Pakhomov, M. M. Ovchinnikov, S. D. Khizhnyak, O. A. Roshchina, P. V. Komarov*, Polym. Sci., Ser. A***,** 2011, **53**, 1574-1581.
3. M. M. Ovchinnikov, S. D. Khizhnyak, M. V. Lavrienko, I. B. Malakhaev, P. M. Pakhomov, *J. Phys. Chem.,* 2005, **79**, 51-53.
4. O. A. Baranova, N. I. Kuzmin, T. I. Samsonova, I. S. Rebetskaya, O. P. Petrova, P. M. Pakhomov, S. D. Khizhnyak, P. V. Komarov, M. M. Ovchinnikov, *Fibre Chem*, 2011, **3**, 74-86.
5. V. G. Alekseev, A. N. Semenov, P. M. Pakhomov*, Russ. J. Inorg. Chem*., 2012, 57, 1041–1044.

6. S. D. Khizhnyak, P. V. Komarov, M. M. Ovchinnikov, L. V. Zherenkova and P. M. Pakhomov, *Soft Matter*, 2017, **13,** 5168-5184.

7. Y. Cui, Y. Wang, L. Zhao, *Small*, 2015, **11**, 5118-5125.

8. G. Socrates, *Infrared characteristic group frequencies: tables and charts,* New York*:* Wiley, 1994.

9. H. B. Vickery, C. S. Leavenworth, *J. Biol. Chem.*, 1930, **86**, 129-143.

10. ImageJ; https://imagej.net/W (accessed November 2021).

11. A. D. Becke, *J. Chem. Phys*., 1988, **88**, 2547.

12. C. Lee, W. Yang, R. G. Parr, *Phys. Rev. B.,* 1988, **37**, 785.

13. B. Delley, *J. Chem. Phys*., 1990, **92**, 508.

14. B. Delley, *J. Chem. Phys.*, 2000, **113**, 7756.

15. M. J. Frisch, G. W. Trucks, H. B. Schlegel, et al., Gaussian 09 (Revision E 0.1 SMP), Wallingford CT: Gaussian Inc. 2009.

16. L. O. Andersson, *J. Polym. Sci.*, 1972, **10**, 1963–1973.

17. H. Sun, *Macromolecules*, 1995, **28**, 701-712.

18. T. Steiner, *Angew. Chem. Int. Ed*., 2002, **41**, 48–76